PROCEEDINGS OF SCIENCE

# Time and Target Field Density Dependent Modelling of Hadronic and Leptonic Processes in Blazar Jets

**Marcel Schroller,**[a,b,*] **Julia Becker Tjus**[a,b,c] **and Lukas Merten**[a,b]

[a] *Theoretical Physics IV, Plasma Astroparticle Physics*
*Faculty for Physics and Astronomy, Ruhr University Bochum, 44780 Bochum, Germany*
[b] *Ruhr Astroparticle and Plasma Physics Center (RAPP Center), Germany*
[c] *Department of Space, Earth and Environment*
*Chalmers University of Technology, 412 96 Gothenburg, Sweden*

*E-mail:* marcel.schroller@ruhr-uni-bochum.de

Active galactic nuclei (AGN), and the accompanied jets, are candidates for the engine of ultra-high-energy cosmic rays, gamma rays, and neutrinos. In 2017, IceCube observed an extragalactic high-energy neutrino event with a strong hint of a directional coincidence with the position of a known jetted AGN TXS0506+056. A deep understanding of the processes related to jets will fuel the field of high-energy cosmic rays, fundamental plasma, astro, and particle physics. However, an AGN jet's physical and mathematical modelling is challenging, with ambiguous signatures that need to be understood by numerical simulations of cosmic-ray transport and interactions.
In this context, we present a simulation framework for hadronic constituents and their interactions inside a plasmoid propagating along the AGN jet axis. Consequently, with the ability to fully resolve particle propagation in three spatial dimensions, the framework was utilised to investigate the impact of spacetime-dependent photonic and hadronic target fields on hadronic interactions. In addition, we discuss the time dependence of these interactions and the resulting secondary particle spectra from blazar jets. Furthermore, we will present the results of our simulations and discuss how to implement non-linear leptonic radiation processes into our test particle simulation framework. This will enable us to construct an improved physical description of AGN jets with spatially and temporally resolved interactions inside them.
This work is supported by the DFG (SFB 1491)

38th International Cosmic Ray Conference (ICRC2023)
26 July - 3 August, 2023
Nagoya, Japan


*Speaker





PoS(ICRC2023)1589

## 1. Introduction

High-energy neutrinos, as measured by the IceCube observatory in the past few years, are tracers of hadronic interactions and, thus, can be used to close in on the origin of ultra-high-energy cosmic rays (UHECRs) and their acceleration sites [1, 2]. AGN, particularly the AGN-subclass of blazars, have been in discussion as potential sources for UHECRs for a long time[3–5, 7, 8].
Numerical calculations can help to disentangle the connections between the individual messengers. There are several numerical frameworks for the simulation of leptohadronic processes in a generic AGN-jet environment in development to this date, e.g. the AM$^3$-code [13], the PARIS code [14] or the ATHE$\nu$A-framework. Those codes are designed to integrate the transport equation numerically and include different models regarding radiative energy loss processes, secondary particle production and radiation for one-zone problems and 1-dimensional steady-state solutions. They have been successfully applied to various problems related to AGN jets, e.g. the modelling of spectral energy distributions or calculating the temporal structure of photon lightcurves [13–15].
Recently, a new code for the propagation of high-energy particles in relativistic plasmoids has been developed by [9], which was achieved by modifying the CRPropa-framework[1]. This can be utilized to simulate ballistic propagation in a test particle approach, as well as diffusive transport via pseudo-particle propagation of high-energy protons along an AGN-jet axis. The primary particles are imposed with interactions with spacetime-dependent photon and proton target fields, linked with the ability to resolve the propagation in three spatial dimensions fully. Thus, the framework is able to investigate multi-messenger spectra without further simplifying assumptions regarding escape time scales, which was explicitly shown in [16]. Further, it was hypothesized that the production of high-energy neutrinos in hadronic interactions occurs while the gamma-ray activity of the blazar is deficient [12]. This idea is supported by an anti-correlation between gamma-rays and radio emission at the detection time of the high-energy neutrino [12].
In contrast, radio flux and gamma-rays at other times seem to correlate somewhat. Precisely this phenomenon can be observed using the modified version of CRPropa as shown in [17], where an AGN flare was modelled from a relativistic plasmoid containing high-energy protons. However, it has to be kept in mind that the full resolution of test particle trajectories and the calculation of the respective particle interactions comes with the price of high computational costs in comparison to integrative methods.

In this paper, we want to discuss further the advantageous properties of this framework and how to include second-order leptonic interactions for an improved model of plasmoids in AGN jets.

## 2. Simulation Setup

The simulations have been created by significantly modifying the CRPropa framework[10] to work in a local source environment, in which a plasmoid is assumed at rest, and the AGN environment is passing by the plasmoid in relativistic motion. A final change of reference frame provides the particle spectra in the observer's frame [9]. In this framework, the particles can either be propagated by solving the equation of motion, representing a ballistic approach, or via the solution of the transport equation, implemented into the CRPropa framework by using the method

[1]CRPropa v3.2 [10]

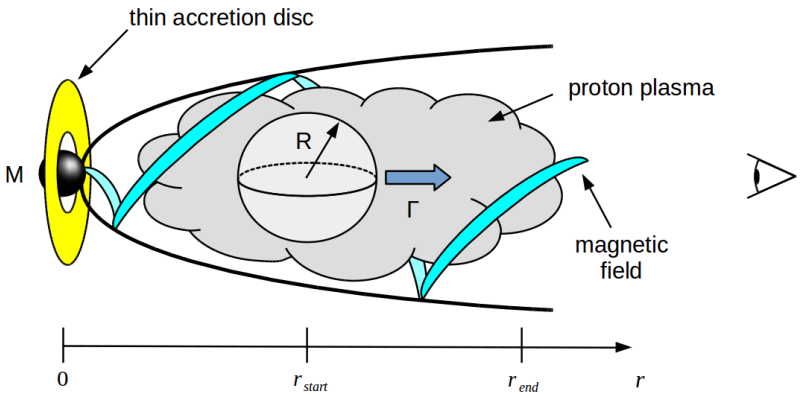


**Figure 1:** The abstract simulation scheme, with plasmoid of radius $R$, bulk Lorentz factor $\Gamma$, central engine with thin accretion disk, as well as the jet structure, depicted as a cone. The jet is assumed to contain a relativistic plasma and a Kolmogorov-turbulent magnetic field. Taken from [9].

of Stochastic Differential Equations. In [9], first results using the ballistic approach for particles with $10^8$ GeV have been presented. The simulation starts with the homogeneous injection of a fixed number $N_p$ of protons into a spherical region with radius $R$, hereafter referred to as *plasmoid*. The energy of the protons will either be monochromatic or power-law-like distributed with spectral index $\alpha_p$ and the injection is instantaneous in time at some starting point $t_0$.

The plasmoid itself will start propagating at a defined distance $r_0$ from the central engine, the SMBH or SMBBH, with bulk Lorentz factor $\Gamma$. A thin accretion disk will illuminate the plasmoid, resembling a thermal black body field and is Doppler de-boosted inside the plasmoid's rest frame. After travelling a pre-defined distance $d = r_{\text{end}} - r_0$, the simulation will terminate.

Furthermore, the jet, which is launched from the AGN, will contain a relativistic plasma, hadronic and leptonic, which is permeated by a purely Kolmogorov-turbulent magnetic field with correlation length $l_c$ and mean-field strength at the base of the jet, $B_0$. The turbulent field is designed to deflect all ambient charged particles to isotropize their direction of momenta in a few simulation steps.

Besides the deflection, ambient electrons contribute to the interactions with their isotropic synchrotron emission during their gyration around the magnetic field lines. The hadronic component of the relativistic plasma serves as a target for proton-proton scattering inside the plasmoid. Ambient protons are designed as a scalable matter field in the sense of space- and time-dependent interactions.

Energetically, the magnet field and ambient plasma are designed to be in equipartition:

$$U_B = \frac{B^2}{2\mu_0} \stackrel{!}{=} U_{\text{particles}} = U_p + U_e, \tag{1}$$

with the vacuum permeability $\mu_0$ and the respective particle energy densities $U_p$ and $U_e$ for protons and electrons. For a detailed discussion about all scaling functions implied in this model description, see [9].

| Parameter | Value |
|---|---|
| Proton energy $E_\mathrm{p}$ | $10^5\,\mathrm{GeV} - 10^8\,\mathrm{GeV}$ |
| Plasmoid radius $R$ | $10^{13}\,\mathrm{m}$ |
| Plasmoid Lorentz factor $\Gamma$ | 10 |
| Magnetic field: Initial RMS value $B_0$ | 1 G |
| Magnetic field: Turbulence & spectral index $\alpha$ | Kolmogorov-type, $\alpha = -5/3$ |
| Magnetic field: Correlation length $l_c$ | $(2/3) \cdot 10^{11}\,\mathrm{m}$ |
| Magnetic field: Grid points | $(512)^3$ |
| Magnetic field: Spacing $\Delta s_G$ | $R/(256 \cdot 32 \cdot 2)$ |
| Magnetic field: $l_\mathrm{min}$ | $2\Delta s_G$ |
| Propagation module (CRPropa intern): Ballistic | PropagationBP |
| Propagation module (CRPropa intern): Diffusive | DiffusionSDE |

**Table 1:** Simulation parameters, given in the rest frame of the plasmoid. All simulations are performed in a modified version of CRPropa 3.1 as presented in Hörbe et al. in [9] with further additions made for this paper as described above. The numerical requirements for the magnetic field are derived from [11].

## 3. Lepto-Hadronic Processes

This section shall introduce the various interactions of our simulation framework. The subscript *PF* denotes a generic photon, which is initialized through the tabulated files of photon fields as described in [9] Synchrotron radiation of a charged nucleus $N$ (lepton $l$):

$$N\,(l) \rightarrow N'\,(l') + \gamma_\mathrm{synch}. \tag{2}$$

The Bethe-Heitler pair-production [18]:

$$N + \gamma_\mathrm{PF} \rightarrow N' + e^+ + e^-. \tag{3}$$

Nuclear decay is performed for nuclei, not for mesons or baryons other than neutrons:

$$M \rightarrow N + X. \tag{4}$$

Photo-Pion production simulates multi-pion-production from photohadronic interactions using the SOPHIA event generator developed by Mücke et al. [19]:

$$N + \gamma_\mathrm{PF} \rightarrow X + n_0\pi^0 + n_+\pi^+ + n_-\pi^- \tag{5}$$

Secondary mesons are not propagated in our framework but decay instantly into their stable products, gamma-rays, electrons/positrons and (anti-)neutrinos, depending on the educt. Proton-proton scattering results as well in multi-pion-production for the interaction of a primary high-energy proton $p$ with a background proton, which is defined as proton a proton target field density, following the parametrization of energy spectra of secondary particles from proton-proton scattering, calculated by Kelner et al.[21]:

$$p + p_\mathrm{Background} \rightarrow p' + p'_\mathrm{Background} + n_0\pi^0 + n_+\pi^+ + n_-\pi^- \tag{6}$$

Gamma-ray interactions with the background photon field are based on the Breit-Wheeler process [20], where in dependence on the centre-of-mass energy, up to three electron-positron pairs are generated:

$$\gamma + \gamma_{\mathrm{PF}} \rightarrow ne^{+} + ne^{-} \qquad n \in \{1, 2, 3\} \tag{7}$$

Inverse Compton-scattering of a charged lepton $l$ can be invoked for generic background fields:

$$l + \gamma_{\mathrm{PF}} \rightarrow l' + \gamma \tag{8}$$

## 4. Time and Density Dependence

The Space-time dependence of our target field densities for interactions and propagation is managed over a 4-dimensional grid. Generally, these dependencies can only be invoked if the interaction is linearly scalable by any means, or alternatively, if the interaction rate $\tau$/ the inverse interaction length $\lambda^{-1}$ can be expressed like

$$\tau\left(\vec{x}, t\right) = \lambda^{-1}\left(\vec{x}, t\right) = \sigma \cdot \phi_I\left(\vec{x}, t\right), \tag{9}$$

$$\phi_I\left(\vec{x}, t\right) = \phi_0 \cdot \phi\left(\vec{x}, t\right), \tag{10}$$

with the static cross-section $\sigma$ of the given interaction and an interaction field $\phi_I\left(\vec{x}, t\right)$, which can be further split into a part, which defines the initial conditions, $\phi_0 \equiv$ const. and the actual scaling, $\phi\left(\vec{x}, t\right)$. The scaling function eq. (9) can be of arbitrary shape in space and time, in order to de- or increase the strength of interactions depending on position and elapsed propagation time in the plasmoid's rest frame.

Following this approach, we can calculate the primary and secondary particle fluxes leaving our plasmoid in its rest frame. This was done for a simulation with space-time dependent interactions and environment as well as for an isotropic constant one, with the same initial conditions but otherwise stationary. In Figure 2 we show the quotient of primary and secondary particle flux leaving through the plasmoid's surface. For propagation distances greater than $D \approx R_{\mathrm{plasmoid}} = 10^{13}$ m, the particle fluxes deviate significantly from each other. This results in an underestimation of the high-energy CR-flux escaping the plasmoid (blue marker for protons, yellow marker for neutrons, violet marker for nucleons altogether) and an overestimation of secondary messengers, gamma-rays and neutrinos (green and red marker, respectively) from interactions described in section 3 for later times in the evolution of the plasmoid if the target fields are assumed to be isotropic and constant.

## 5. Implications for Multi-Messenger Emission

In addition, we can use our framework to investigate the impact of propagation regimes on the emission of high-energy protons, gamma-rays and neutrinos from plasmoids in AGN jets. A thorough analytical and numerical discussion of the different propagation regimes and their effect on multi-messenger emission is presented in our previous work [16]. Here we want to highlight the findings of the numerical simulations using our framework and refer to the paper mentioned above for a detailed discussion.

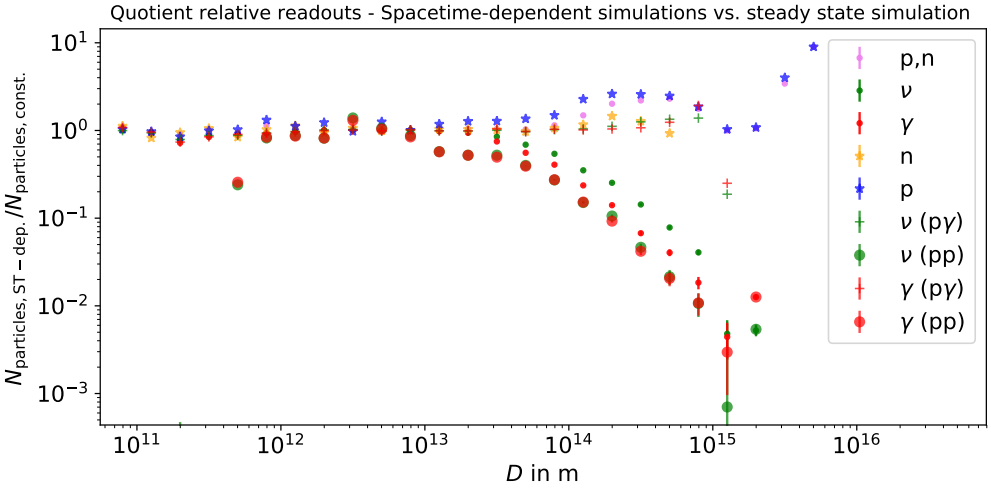


**Figure 2:** Quotient of primary and secondary particle flux at the plasmoid's surface of a spacetime-dependent environment and an isotropic constant environment, fixed at the launching position of the plasmoid. Parameter setup as described in 1, scalings and target fields following [9].

Accordingly, the simulation setup follows the scheme and parameter space described in Section 2 and Table 1. First, we simulated the cosmic ray flares in a ballistic approach by solving the equation-of-motion of protons affected by the Lorentz force in the turbulent magnetic field numerically and derived the steady-state diffusion coefficients by applying the Taylor-Green-Kubo formalism [22] to our particle trajectories. In order to stress how crucial it is to consider the correct propagation regime, we naively extrapolated a diffusion coefficient to higher energies from low-energy data.

Figure 3(a) shows the flaring behaviour for a monochromatic energy flare at $E = 10^5$ GeV. The diffusive description (orange downward triangle) shows a substantial enhancement concerning the equation-of-motion approach (blue upward triangle) at early times below $10^3$ s, in accordance with our findings in [16]. The behaviour of $\mathrm{d}N/\mathrm{d}t$ is similar for both approaches, with a slight shift explained by the uncertainties in our numerical determination of the diffusion coefficient used for the diffusive approach. In the diffusive transport regime for a constant diffusion coefficient, we expect $\langle \Delta x \rangle \propto t^{1/2}$. This results in the differential particle number $\mathrm{d}N/\mathrm{d}t \propto t^{-1/2}$ of escaping particles. Note that the decrease in the number of remaining particles in the plasmoid leads to a strong cut-off at large times due to the steady escape. Since, in the diffusive approach, more particles initially leave the plasmoid, the particle density in the plasmoid is lower than in the equation-of-motion approach, so an earlier cut-off is visible.

Figure 3(b) shows the flare for diffusive (again orange downward triangle) and equation-of-motion (again blue upward triangle) behaviour at $10^8$ GeV. Here, there is an apparent difference between the two flares, with the diffusive approach yielding a dominant contribution at early times. In contrast to the diffusive regime with $\mathrm{d}N/\mathrm{d}t \propto t^{-1/2}$, we expect a constant differential particle number for the ballistic transport regime with $\langle \Delta x \rangle \propto t$. The initial slight drop for the equation-of-motion may be explained by statistical deviations from the initial homogeneous particle distribution in the plasmoid, especially when slightly more particles are in the outer spheres of the plasmoid at $t = 0$. Since, in the diffusive case, significantly more particles initially leave the plasmoid,

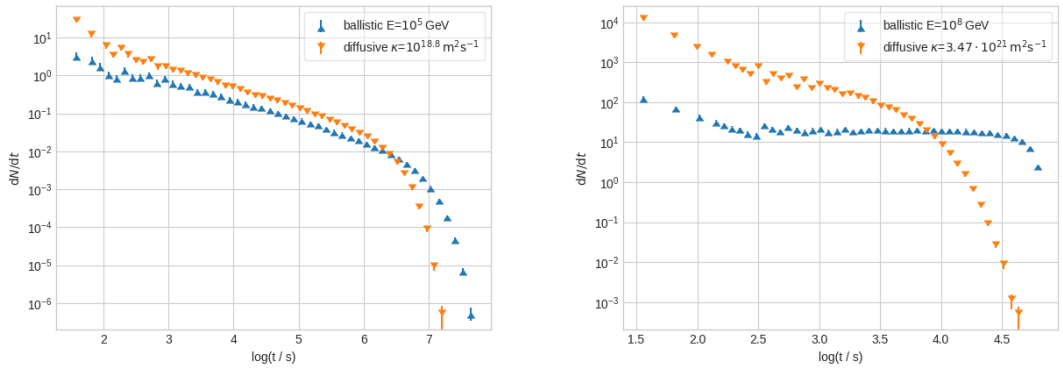


(a) (b)

**Figure 3:** Cosmic-ray flare of protons with $E_\mathrm{p} = 10^5$ GeV (*Panel (a)*) and $E_\mathrm{p} = 10^5$ GeV (*Panel (b)*) from a blazar in the diffusive propagation model (orange downward triangle) and in comparison in the ballistic propagation model (blue upward triangle) as differential particle number per unit time $\mathrm{d}N/\mathrm{d}t$ over time. The number of injected particles is $N_\mathrm{inj} = 10^5$.

the particle density in the plasmoid is much lower than in the equation-of-motion approach, so a cut-off is visible much earlier in the diffusive approach. Thus, these test simulations emphasize the importance of propagating the particles in the proper transport regime. Only a thorough analysis, which compares the transport properties, will lead to a prediction that compares the observation of non-thermal emissions from blazars.

## 6. Second-order Leptonic Processes

Consequently, to model multi-messenger signatures of high-energy protons and leptons in AGN-jets, self-interactions of the constituents are crucial to consider. The next step to a more consistent framework is to include the most dominant second-order leptonic radiation processes for high-energy gamma-ray physics, synchrotron self-absorption and synchrotron self-Compton processes. Since we are operating in a highly parallelized framework for our test particle simulations, self-interactions of our simulated particles are generally excluded.

However, the simulation time steps can be split into independent test particle simulations. Between pre-defined time steps on another simulation time scale, one can calculate the synchrotron radiation of the electron population (primary and secondary) and the interaction with background photon fields self-consistently in an external framework. The resulting distributions can then be used to update the target fields and pair distribution, which is ultimately used to sample and derive the constituents and photon targets for the next simulation step in the test particle picture. Finally, after superimposing the results of each iteration, we can calculate the resulting light curves and spectra of our plasmoid spatially and temporally resolved.

## References


[1] Aartsen et al. Advances in Space Research 62.10 (2018): 2902-2930.

[2] Biermann, P. L. and Strittmatter, P. A. The Astrophysical Journal 322 (1987): 643.

[3] Stecker, F. D. Physical Review D 72.10 (2005): 107301.

[4] Nellen, L., Mannheim, K. and Biermann, P. L. Physical Review D 47.12 (1993): 5270.

[5] Mannheim, K. Astroparticle Physics 3.3 (1995): 295-302.

[6] Merten L., et al. Journal of Cosmology and Astroparticle Physics 2017.06 (2017): 046.

[7] Murase, K., Oikonomou, F. and Petropoulou, M. ApJ 865.2 (2018): 124.

[8] Becker Tjus, J. and Merten, L. Physics Reports 872 (2020): 1-98.

[9] Hoerbe M. R., et al. MNRAS 496.3 (2020): 2885-2901.

[10] Alves Batista R., et al. Journal of Cosmology and Astroparticle Physics 2022.09 (2022): 035.

[11] Reichherzer P., et al. MNRAS 498.4 (2020): 5051-5064.

[12] Kun E., et al. The Astrophysical Journal Letters 911.2 (2021): L18.

[13] Gao, S., Pohl, M. and Winter, W. The Astrophysical Journal 843.2 (2017): 109.

[14] Cerruti M., et al. MNRAS 448.1 (2015): 910-927.

[15] Dimitrakoudis, S., et al. Astronomy & Astrophysics 546 (2012): A120.

[16] Becker Tjus, J., et al. Physics 4.2 (2022): 473-490.

[17] Schroller et al. PoS(ICRC 2021)

[18] Bethe, H., and Heitler, W. Proceedings of the Royal Society of London 146.856 (1934): 83-112.

[19] Mücke, A., et al. Computer Physics Communications 124.2-3 (2000): 290-314.

[20] Breit, G., Wheeler, J. A., Physical Review 46.12 (1934): 1087.

[21] Kelner, S. R., et al. Physical Review D 74.3 (2006): 034018.

[22] Kubo R. Journal of the physical society of Japan 12.6 (1957): 570-586.


PoS(ICRC2023)1589